# Whole-Body Diffusion-Weighted MRI: Tips, Tricks, and Pitfalls

Dow-Mu Koh[1]
Matthew Blackledge[2]
Anwar R. Padhani[3]
Taro Takahara[4]
Thomas C. Kwee[5]
Martin O. Leach[2]
David J. Collins[2]

**OBJECTIVE.** We examine the clinical impetus for whole-body diffusion-weighted MRI and discuss how to implement the technique with clinical MRI systems. We include practical tips and tricks to optimize image quality and reduce artifacts. The interpretative pitfalls are enumerated, and potential challenges are highlighted.

**CONCLUSION.** Whole-body diffusion-weighted MRI can be used for tumor staging and assessment of treatment response. Meticulous technique and knowledge of potential interpretive pitfalls will help to avoid mistakes and establish this modality in radiologic practice.

Extracranial diffusion-weighted MRI (DWI) is increasingly used for disease evaluation in oncology [1]. DWI depicts differences in the mobility of water in tissues. Cellular tumors exhibit greater impeded water diffusion, reflected as high signal intensity on images with high b values, and return lower apparent diffusion coefficient (ADC) values [2, 3]. This mechanism of image contrast generation is being harnessed in clinical practice and in research for detecting malignancy in different tumor types and organ systems to inform tumor staging and management decisions.

DWI can be performed relatively quickly with a free-breathing spin-echo echo-planar technique [1, 4]. Advances in magnet design, receiver coil technology, and acquisition mean that DWI can be performed over multiple imaging stations in a relatively short time. The concept of whole-body imaging with DWI was initially proposed by Takahara et al. in 2004 [5]. Those authors described whole-body DWI with background signal suppression. Since then, interest in advancing the utility of the technique has continued to grow, particularly in the field of oncologic imaging.

The idea of whole-body MRI acquisition in multiple image stacks of the entire body is not new. In the 1990s, whole-body MRI with conventional T1-weighted and STIR sequences was proposed and investigated for tumor detection [6–8]. These studies had relatively high sensitivity, specificity, and diagnostic accuracy for visualization of a variety of tumor types [6, 7, 9–12]. However, whole-body MRI has not gained widespread adoption despite its apparent usefulness. One of the negative factors was likely the relatively long examination time. Typically, these studies took 1 hour or longer to perform and resulted in a multitude of images, which posed challenges for image viewing and interpretation before sophisticated workstations became available.

Since the initial studies, substantial improvements have been made in MRI hardware design and software, which allow performance of multipart MRI examinations with relative ease [13, 14]. The advent of continuous moving table technology allows even more efficient image acquisition [12, 13, 15, 16]. Dedicated workstation software also streamlines onsite and remote viewing of whole-body datasets. These software tools are furnished with pushbutton functions that stitch together images acquired at different anatomic stations and displayed as a single image to facilitate reading. Whole-body DWI was developed amid these innovations, making it possible to add DWI to conventional whole-body imaging protocols. With modern state-of-the-art MRI systems, whole-body MRI from vertex to the midthigh (analogous to the coverage for a typical body PET/CT examination) can be accomplished with T1-weighted, fat-suppressed T2-weighted, or STIR and DWI sequences in 40–60 minutes, making it a viable tool for clinical deployment. For this article, an understanding of the basic principles of DWI is assumed and is not discussed. A number of review articles are available [1–3, 17, 18].

**Keywords:** diffusion-weighted imaging, MRI, oncology, pitfalls, technique, whole body

DOI:10.2214/AJR.11.7866

Received August 29, 2011; accepted after revision January 2, 2012.

[1]Department of Radiology, Royal Marsden Hospital, Downs Rd, Sutton, Surrey SM2 5PT, UK. Address correspondence to D. M. Koh (dowmukoh@icr.ac.uk).

[2]CRUK-EPSRC Cancer Imaging Centre, Institute of Cancer Research, Surrey, UK.

[3]Paul Strickland Scanner Centre, Middlesex, UK.

[4]Tokai University School of Medicine, Kanagawa, Japan.

[5]University Medical Center Utrecht, Department of Radiology, Utrecht, The Netherlands.

*AJR* 2012; 199:252–262

0361–803X/12/1992–252

## Clinical Impetus for Whole-Body Diffusion-Weighted MRI

There has been a resurgence of interest in whole-body MRI, stimulated in part by clinical needs and concerns about radiation safety in CT [19, 20]. Ionizing radiation from CT studies can result in a substantial increase in the lifetime risk of cancer [19]. As a result, CT manufacturers have responded by designing more efficient CT systems that will reduce radiation exposure for each study. Another option, however, is radiation avoidance by performing MRI instead of CT when appropriate, as in the care of young adults and children [21].

From the clinical perspective, there is emerging evidence that whole-body MRI may be a solution to current unmet needs in cancer staging. A difficult area in tumor evaluation has been assessment of metastatic bone disease and the response to hormonal, chemotherapeutic, and radiation treatment. The difficulty arises because bone disease confined to the marrow cavity is not considered measurable according to conventional measurement criteria (e.g., the Response Evaluation Criteria in Solid Tumors) [22], although measurement criteria have been proposed for bone disease associated with a soft-tissue component [23].

The most widely prescribed imaging test for evaluation of bone disease is radionuclide bone scintigraphy with technetium-labeled tracers. However, the results can be false-negative in patients with active bone disease because lytic bone diseases may not induce an osteoblastic reaction [24, 25]. Furthermore, there is a global shortage of the $^{99m}$Tc isotope used for bone scintigraphy due to uncertainty over its supply [26]. The search is ongoing for an imaging technique to fill this gap. Although it is possible to replace $^{99m}$Tc-radiolabeled bone scintigraphy with $^{18}$F-labeled PET/CT [24], it is unlikely that there will be sufficient numbers of PET/CT scanners worldwide to cope with the workload and demand. Whole-body MRI is poised to become a viable alternative. Studies of whole-body MRI have shown high diagnostic sensitivity, compared with bone scintigraphy and FDG PET/CT, for detecting bone metastasis [6, 9, 24, 27–32].

Literature findings [33–35] suggest that whole-body MRI that includes DWI can be developed to detect diagnostic and response

**TABLE 1: Selected Studies of Whole-Body Diffusion-Weighted MRI (DWI) for Varied Indications**

| Study | Year | No. of Patients | Whole-Body MRI Technique | Comparison Modality | Findings |
|---|---|---|---|---|---|
| Lymphoma | | | | | |
| van Ufford et al. [36] | 2011 | 22 | DWI, STIR and T1-weighted | FDG PET/CT | 77% concordance with PET for staging; whole-body DWI understaging rate was 0% but overstaging, 23% (5/22) |
| Lin et al. [38] | 2011 | 15 | Respiratory-gated DWI | FDG PET/CT | ADC increased in nodes after chemotherapy; use of ADC and size criteria reduced false-positive rate for residual nodal masses |
| Lin et al. [39] | 2010 | 15 | Respiratory gated DWI | FDG PET/CT | 90% sensitivity, 94% specificity in assessment of nodal involvement by size; 81% sensitivity, 100% specificity with ADC and size criteria |
| Kwee et al. [49] | 2009 | 31 | DWI | CT | DWI similar to CT for disease staging |
| Mixed disease | | | | | |
| Fisher et al. [60] | 2011 | 68 | T2-weighted and DWI | FDG PET/CT | High detection rate and PPV with T2-weighted DWI, evaluated side by side (72%, 89%) and by fusion (74%, 91%) |
| Gutzeit et al. [44] | 2010 | 36 | DWI | FDG PET/CT | DWI had higher sensitivity (97%) than PET/CT (91%) for patients with > 10 skeletal lesions |
| Nakanishi et al. [52] | 2007 | 30 | DWI, STIR, T1-weighted | Bone scintigraphy, CT | STIR and T1-weighted DWI had higher sensitivity (96%) and PPV (98%) than bone scintigraphy and whole-body MRI without DWI |
| Malignant melanoma | | | | | |
| Laurent et al. [40] | 2010 | 35 | T1-weighted, STIR, and DWI | FDG PET/CT | 82% sensitivity, 97% specificity for DWI; 73% sensitivity, 93% specificity for PET/CT |
| Breast cancer | | | | | |
| Heusner et al. [43] | 2010 | 20 | DWI | FDG PET/CT | 91% sensitivity, 72% specificity for DWI; 94% sensitivity, 99% specificity for PET/CT |
| Lung cancer | | | | | |
| Chen et al. [46] | 2010 | 56 | DWI | FDG PET/CT | Lymph node metastasis: 91% sensitivity, 90%, specificity for DWI; 98% sensitivity, 97% specificity for PET/CT. Other metastases: 90% sensitivity, 95% specificity for DWI; 98% sensitivity, 100% specificity for PET/CT |
| Takenaka et al. [47] | 2009 | 115 | DWI, T1-weighted, STIR | FDG PET/CT, $^{99m}$Tc bone scintigraphy | Specificity and accuracy of whole-body MRI with DWI significantly better than scintigraphy for bone metastasis |
| Ohno et al. [50] | 2008 | 203 | DWI, T1-weighted, STIR | FDG PET/CT | Accuracy of whole-body-MRI with DWI ($A_z$, 0.87) similar to that of PET/CT ($A_z$, 0.89). |

Note—ADC = apparent diffusion coefficient, PPV = positive predictive value, $A_z$ = area under the curve.

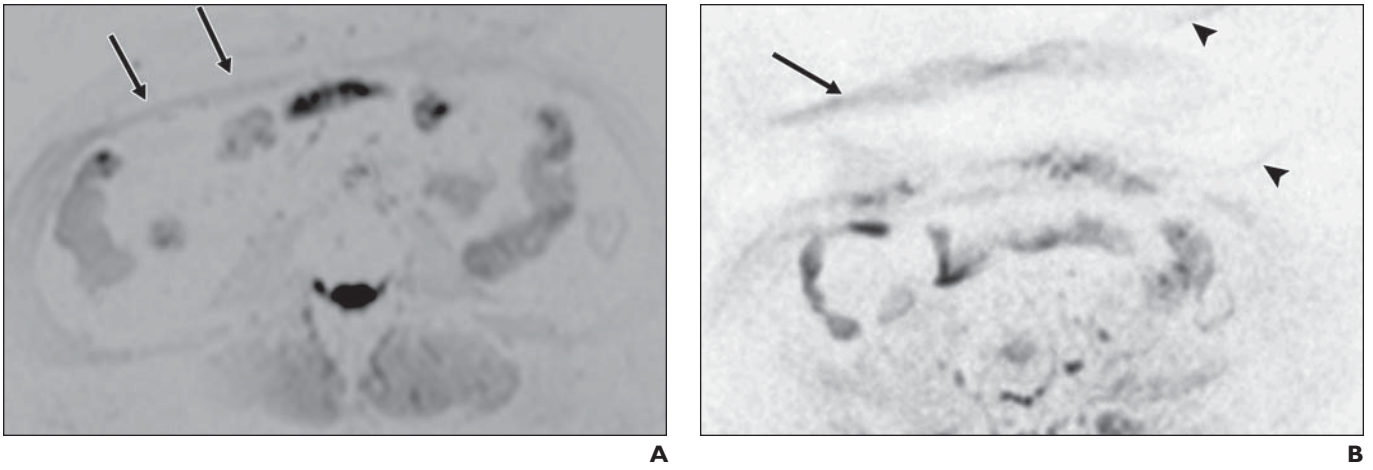

**Fig. 1**—45-year-old healthy man. Potential problems with diffusion-weighted MRI at 3 T.
**A,** Diffusion-weighted MR image (b = 750 s/mm$^2$) shows eddy current–induced geometric distortion (*arrows*) resulting in distorted appearance of right anterior abdominal wall.
**B,** Diffusion-weighted MR image (b = 750 s/mm$^2$) shows Nyquist ghosting artifact (*arrowheads*). Arrow indicates area of distortion in **A.**
**C,** Sagittal 3-T MRI reformats of three image stacks (b = 750 s/mm$^2$) show misalignment of spine (*arrows*).

biomarkers of malignant bone and soft-tissue diseases. Table 1 summarizes selected studies on the use of whole-body DWI for disease staging and response assessment in the care of oncology patients [36–52].

## Implementation of Whole-Body Diffusion-Weighted MRI

The use of MRI for oncologic imaging is continuing to grow. Imaging platforms being introduced have technologies to optimize multistation body imaging that includes DWI. This capability increases the efficiency of sequential imaging at more than one anatomic station without manual repositioning of the patient or the surface receiver coils between acquisitions. We discuss the tips, tricks, and pitfalls of implementing whole-body DWI in current clinical MRI systems. Included are the choice of field strength, patient positioning on the unit, optimization of the imaging sequence, image processing and viewing, and image interpretation.

### *Choice of MRI System: 1.5 T Versus 3 T*

With current technology, whole-body DWI is easier to implement with 1.5-T than with 3-T systems. Whole-body DWI at 3 T is often more difficult because artifacts can be more challenging to control and minimize. In addition to the general issues at 3 T, such as dielectric effects and tissue-specific absorption rates [53, 54], there are challenges related to the DWI measurements. First, eddy currents induced by rapid switching of the magnetic gradient field with echo-planar imaging cause residual magnetization that results in geometric distortion and image shearing [4] (Fig. 1A). This distortion can make it more difficult to register and align DW images with corresponding morphologic T1- and T2-weighted images. Second, because of the greater $B_1$ field inhomogeneity at 3 T, it can be difficult to achieve uniform fat suppression across large fields of view, and the result is chemical-shift and ghosting artifacts (Fig. 1B). Third, because the MR frequency offsets applied can differ markedly between anatomic stations, voxel shift can occur in the phase-encoding direction and cause misalignment of structures (e.g., the spinal cord) between imaging stations (Fig. 1C). The result is difficulty in accurate alignment of individual imaging stations to produce smooth composite images (e.g., whole-body sagittal images), even though images from individual anatomic stations are of high quality. This limitation may not affect the diagnostic quality of the acquired images but falls short of producing pleasing reformatted images for clinicians and patients to review. Coronal reformats are usually less affected because the phase-encoding direction is often anteroposterior.

Despite the limitations, it is clear that imaging at 3 T has the intrinsic advantage of a higher signal-to-noise ratio (SNR), which can enhance lesion detection. As imaging technology continues to improve, a variety of implementations are being explored to minimize eddy current effects and to optimize fat suppression across a large FOV at 3 T. These features are discussed later. Post-processing techniques are being developed for image alignment and registration. In the current state of the art, whole-body DWI technique is more robust at 1.5 T, but it is conceivable that with the current pace of imaging improvement, the technique may soon be equally successful at 3 T.

### *Patient Setup*

The success of a whole-body DWI study relies in part on patient cooperation to minimize movement during the study. As such, patients should be told of the approximate examination time (typically 40–60 minutes) and be warned that the study can be noisy owing to the vibration of the MRI bed. The patient should be offered the opportunity for bladder emptying

**TABLE 2: Typical 1.5-T Diffusion-Weighted Protocol for Whole-Body MRI With Three 1.5-T Systems**

| Protocol | Avanto (Siemens Healthcare) | Intera (Philips Healthcare) | Signa (GE Healthcare) |
|---|---|---|---|
| Imaging plane | Axial | Axial | Axial |
| FOV (cm) | 380 × 380 | 400 × 280 | 440 × 440 |
| Matrix Size | 150 × 256 | 128 × 96 | 128 × 88 |
| TR | 14,000 | 8322 | 6625 |
| TE | 72 | 70 | 64.6 |
| Echo-planar imaging factor | 150 | 37 | |
| Parallel imaging factor | 2 | 2 | |
| No. of signals averaged | 4 | 4 (b = 0), 12 (b = 1000) | 3 |
| Section thickness (mm) | 5 contiguous | 5 contiguous | 8 |
| Direction of motion probing gradients | 3-scan trace | Tetrahedral encoding | |
| Receiver bandwidth | 1800 Hz/pixel | 7.757 (water-fat shift/pixel) | |
| Fat suppression | STIR (inversion time, 180 ms) | STIR (inversion time, 180 ms) | STIR (inversion time, 160 ms) |
| b value (s/mm$^2$) | Typically 0–100 and 600–1000 | 0, 1000 | Single b value, 600 |
| Acquisition time per station | 4 min 30 s | 4 min 2 s | 1 min 28 s |

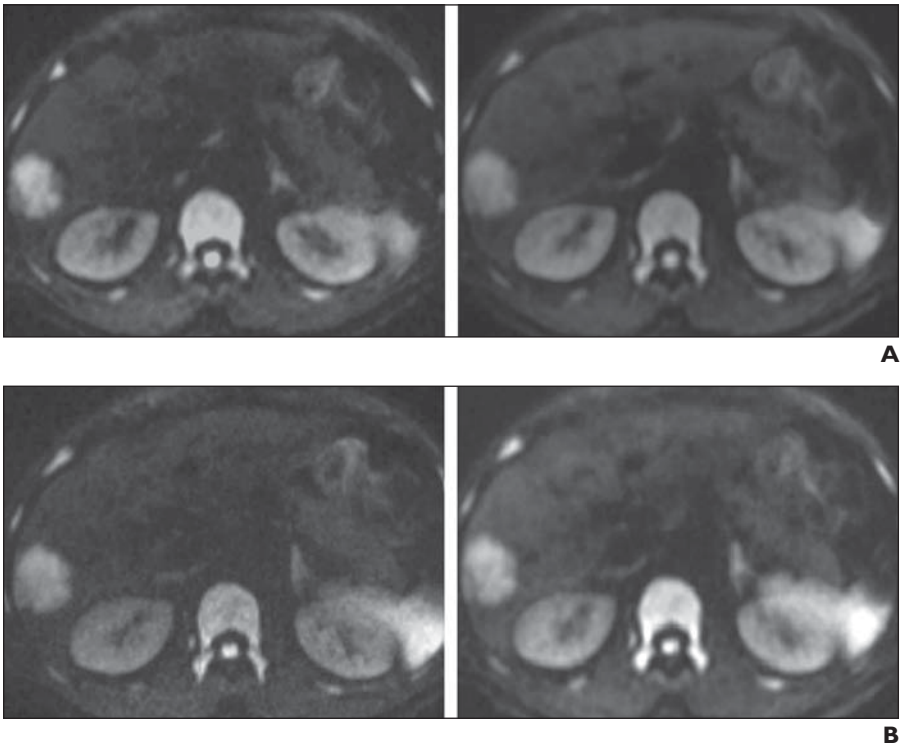


**Fig. 2**—46-year-old man with liver metastasis of colorectal cancer. Example of effects of decreasing TE and matrix size.
**A,** Diffusion-weighted MR images acquired with TEs of 90 ms (*left*) and 76 ms (*right*) with all other imaging parameters equal show use of shorter TE improves signal-to-noise ratio.
**B,** Diffusion-weighted MR images acquired with matrix sizes of 256 × 256 (*left*) and 128 × 128 (*right*) with all other imaging parameters equal shows reducing matrix size improves signal-to-noise ratio.

before the examination to minimize discomfort during the examination.

Many MRI systems are migrating to the use of multiple surface receiver coil arrays deployed over the body to achieve the best SNR. These coils should be deployed contiguously to each other or with a slight degree of overlap (up to 5 cm). Using multiple receiver coil arrays also helps to streamline workflow, improve patient throughput, and minimize examination times. With some older MRI systems, it may be possible to perform whole-body DWI with just a single phased-array receiver coil. Takahara et al. [55] called this method the sliding coil technique. Where surface coils are not available, whole-body DWI can be performed with the receiver elements in the main magnet bore. However, these images have lower spatial resolution and SNR and cannot be acquired with parallel imaging.

The optimum patient setup for a whole-body DWI examination depends on the local MRI hardware configuration, which has a bearing on the efficiency of acquisition and the quality of the images obtained.

### *Imaging Parameters*

The principles of obtaining high-quality whole-body DW images are similar to those for regional examinations. Acquisition and parameter selection should be streamlined to optimize SNR and to minimize artifacts [4]. Table 2 summarizes typical imaging parameters for whole-body DWI with 1.5-T MRI systems from three vendors.

In addition to axially acquired DW images, conventional T1-weighted and STIR and T2-weighted fat-suppressed images are usually obtained in the axial or coronal plane. Breath-hold 3D T1-weighted gradient-echo sequences allow rapid acquisition of T1-weighted images [56]. For assessment of suspected metastatic bone disease, T1-weighted and STIR and T2-weighted fat-suppressed sagittal images of the whole spine are valuable. Coronal DWI acquisitions with higher parallel imaging factors are being evaluated for reducing acquisi-

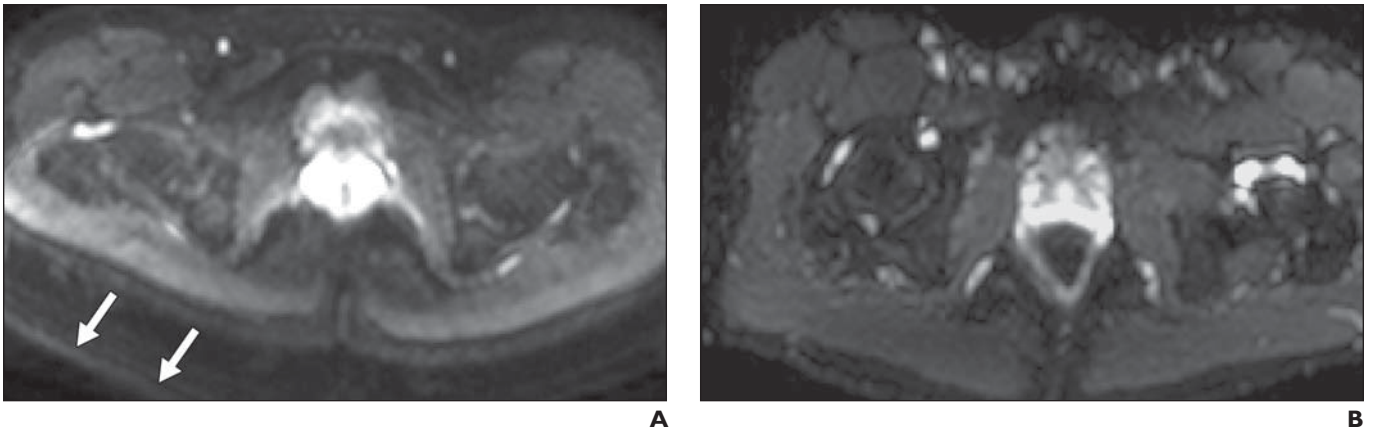

**Fig. 3**—35-year-old healthy man. Example of fat suppression at 3 T.
**A,** Axial STIR fat-suppressed MR image (b = 750 s/mm$^2$) shows substantial chemical-shift ghosting (*arrows*) due to poor fat suppression of posterior abdominal wall.
**B,** Axial MR image (b = 750 s/mm$^2$) acquired with combinatorial fat suppression with spectral attenuated inversion recovery and slice selective gradient reversal shows improvement of fat suppression without marked image artifacts.

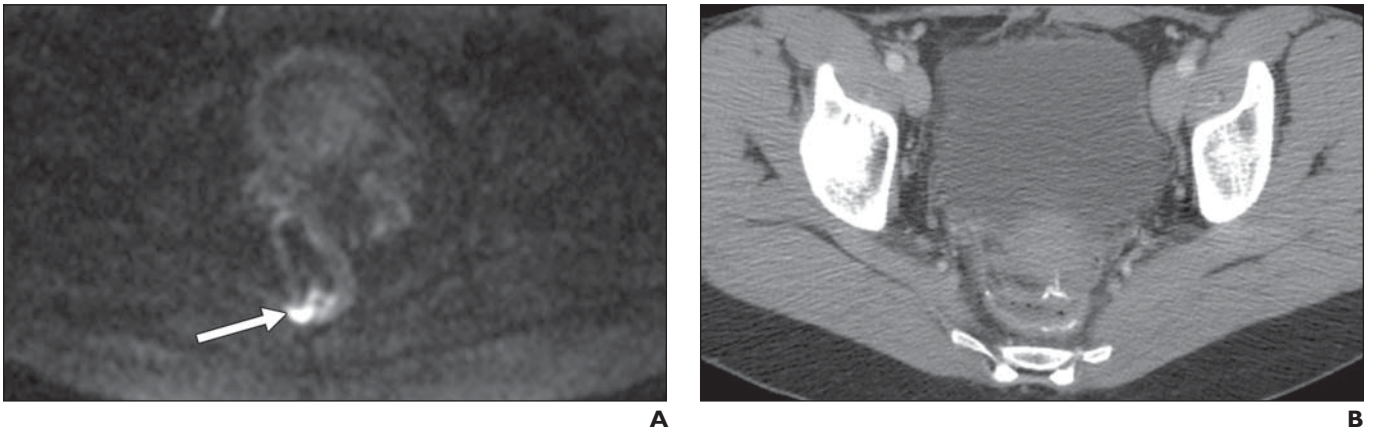

**Fig. 4**—56-year-old woman with history of anterior resection for rectal carcinoma. Example of susceptibility artifacts.
**A,** MR image (b = 900 s/mm$^2$) appears to show area of impeded diffusion (*arrow*) in posterior rectal wall. However, finding is due to susceptibility artifact from surgical material in area.
**B,** CT image shows high-attenuation material related to previous surgery.

tion time to less than 30 minutes. The development of whole-body DWI with continuous table movement may further streamline workflow [16]. With continuous table movement, imaging is always performed in the isocenter of the magnet, avoiding the problem of peripheral field image distortion.

With regard to the choice of b value, two b values usually suffice because increasing the number of b values prolongs examination time. Because the technique is usually used as a contrast mechanism to identify cellular tissues, the higher b value chosen is usually 600–1000 s/mm$^2$. This choice renders the diffusion sequence for the optimal SNR for detecting lesions with ADC values in the range of 500–900 mm$^2$/s, typical of malignancy. The lower b value can be 0–100 s/mm$^2$. Using a lower b value of 50–100 s/mm$^2$ results in vascular signal suppression (black-blood images), which can aid disease detection but at the expense of a longer acquisition time compared with b = 0 s/mm$^2$. When two b values are used, the ADC can be computed for disease quantification or to support image interpretation (e.g., identifying T2 shine-through).

In the performance of DWI, consideration should be paid to maximizing image SNR. One simple rule is to minimize the TE to as low as achievable [4] (Fig. 2). A common error is to use too high a spatial resolution to match those of the morphologic images, leading to lower SNR. Use of lower spatial resolution due to a coarser imaging matrix (e.g., 180 × 180) helps to improve SNR, particularly at higher b values (Fig. 3). When technically possible, free-breathing image acquisition is a robust technique because it allows multiple signal averages, which improve SNR. However, when this technique is suboptimal, multiple breath-hold acquisitions may be considered. Using multiple averaging also allows thinner image partitions (typically 4–5 mm) for multiplanar image reformats [4].

Many types of artifacts can degrade image quality. Common clinical artifacts include poor fat suppression, which results in chemical shift artifacts; eddy current–induced geometric distortions and image shearing; and Nyquist, or N/2, ghosting.

To optimize fat suppression, the use of nonselective fat suppression techniques such as STIR is preferable over chemical-selective sequences such as spectral attenuated inversion recovery, spectral presaturation by inversion recovery (SPIR), and chemical fat suppression over large fields of view [5]. Another method

**TABLE 3: Problems and Suggested Solutions in Body Diffusion-Weighted MRI With Spin-Echo Echo-Planar Technique**

| Problem | Solution |
|---|---|
| Poor signal-to-noise ratio | Use shortest TE achievable |
| | Use multiple averaging method |
| | Choose coarser matrix size |
| | Use thicker partition thickness |
| | Increase FOV |
| | Choose lower b values |
| | Use parallel imaging |
| | Optimize receiver bandwidth |
| Relatively long TE (e.g., > 100 ms) | Try to shorten TE in one of the following ways: |
| | Use simultaneous gradient application schemes (e.g., 3-scan trace) |
| | Increase receiver bandwidth |
| | Use parallel imaging |
| Poor fat suppression and chemical-shift artifact | Use non–chemical-selective fat-suppression scheme over the wide FOV (e.g., STIR) |
| | Increase receiver bandwidth |
| | Use combinatorial fat suppression techniques at 3 T |
| Eddy current effects causing geometric distortion and image shearing | Optimize or increase receiver bandwidth |
| | Use simultaneous gradient application schemes to decrease peak gradient amplitudes |
| Nyquist (N/2) ghosting | Optimize or decrease receiver bandwidth |
| G noise | Reduce parallel imaging factor |
| | Use larger FOV |
| Susceptibility artifacts | Avoid scanning over areas with implants |
| Poor alignment of image stacks between imaging stations | At 1.5 T, omit image shimming and apply center frequency of one imaging station to all subsequent stations |
| | Consider continuous table motion acquisition |
| | Apply software postprocessing |

is spectral-spatial water-only excitation. These approaches may be successful at 1.5 T but still be unsatisfactory at 3 T. Performing DWI at 3 T may require combinatorial fat suppression to ensure uniform fat suppression across the entire FOV [57] (Fig. 4). For example, it may be advantageous to combine STIR with chemical fat suppression (e.g., SPIR). Another fat-suppression technique found useful at 3 T is the slice selective gradient reversal (SSGR) technique [57]. However, use of SSGR, either alone or in combination with STIR imaging, can result in undesired off-resonance signal suppression from water protons (water suppression), which can obscure lesions.

Use of echo-planar imaging, the rapid switching of magnetic gradients, results in residual magnetic fields, which induce eddy currents and cause image distortion. Use of simultaneous gradient application schemes (e.g., three-scan trace and tetrahedral encoding) reduces eddy currents by reducing the peak amplitude of the applied diffusion gradient.

One effective way of dealing with $B_0$-induced distortions is to adjust the receiver bandwidth. The receiver bandwidth is the range of frequencies used to sample the MR signal. Increasing the receiver bandwidth reduces chemical-shift artifacts, decreases the TE of signal acquisition, and reduces geometric distortion, all of which improve image quality. The disadvantages of increasing the receiver bandwidth, however, include reduction of SNR and an increase in Nyquist ghosting (see later). Thus the receiver bandwidth should be adjusted to balance these effects. For DWI of the whole body, the optimal receiver bandwidth is usually much higher than those used for conventional MRI sequences. Typically, a receiver bandwidth of approximately 1600–2000 Hz/pixel is used for body DWI. The receiver bandwidth is expressed differently on different MRI systems. Adjusting the receiver bandwidth may mean changing the receiver bandwidth range (expressed in kilohertz) (GE Healthcare), the water-fat shift (expressed in pixels) (Philips Healthcare), or the receiver bandwidth per pixel (Hz/pixel) (Siemens Healthcare).

The use of echo-planar imaging can result in a sampling artifact, known as Nyquist, or N/2, ghosting. During echo-planar imaging, adjacent lines of k-space are sampled with opposite readout gradients. Misalignment in the sampling from positive and negative gradients leads to additional line modulation in k-space, which is observed as ghosting of the image. Nyquist ghosting can be reduced by applying appropriate phase correction to the data. However, optimizing the receiver bandwidth and echo spacing is also an effective measure.

The common technical issues encountered at body DWI and their solutions are summarized in Table 3. These broad principles should help to guide parameter adjustments in clinical practices.

### *Image Processing and Viewing*

For viewing and reporting of whole-body DWI studies, it is desirable to reformat the

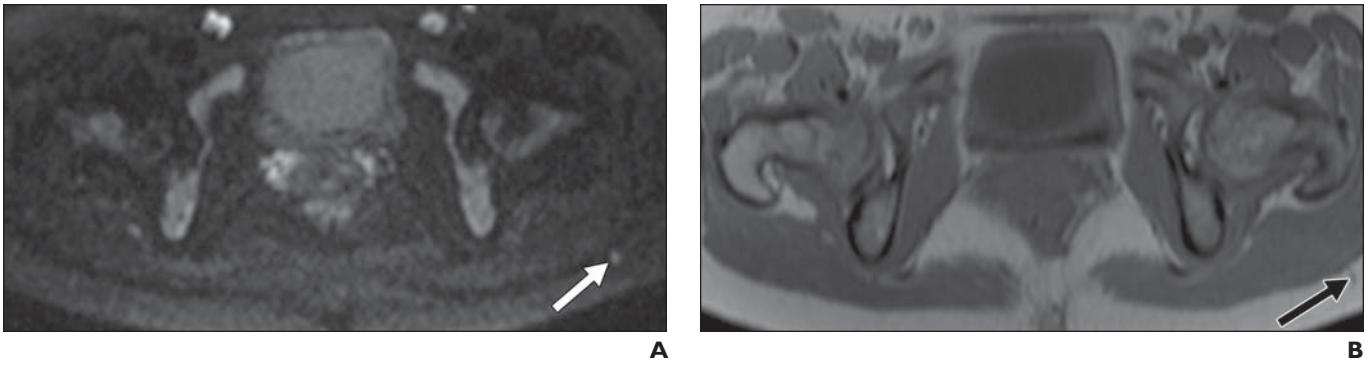

**Fig. 5**—62-year-old woman with history of ovarian cancer.
**A,** MR image (b = 900 s/mm$^2$) through lower pelvis shows focus of impeded diffusion (*arrow*) over left gluteal area.
**B,** MR image shows low-signal-intensity tubular structure (*arrow*) in left gluteal area. Apparent impeded diffusion most likely results from slow flow in presumed small venule.

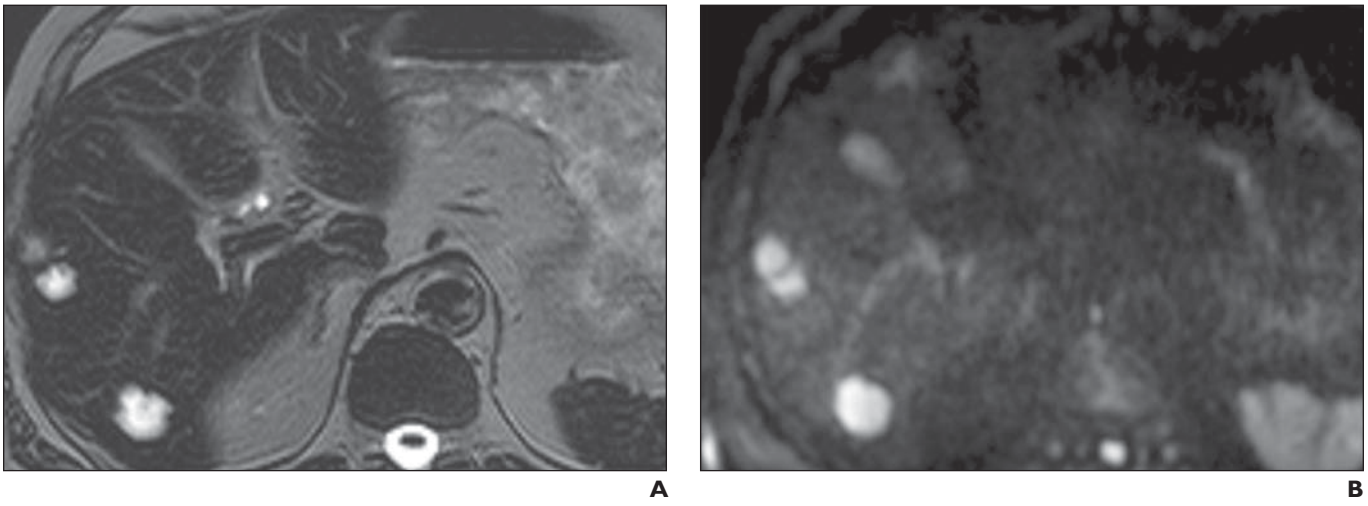

**Fig. 6**—55-year-old man with colorectal liver metastasis. Example of T2 shine-through.
**A,** T2-weighted MR image (TE, 240 ms) shows three high-signal-intensity mucinous metastatic lesions in right lobe of liver.
**B,** MR image (b = 750 s/mm$^2$) shows apparent high signal intensity, suggesting impeded diffusion of metastatic lesions.
**C,** MR image shows high apparent diffusion coefficient of lesions consistent with T2 shine-through effect.

high b value DW images in the axial, coronal, and sagittal planes for multiplanar assessment. Whole-body DW images are usually displayed with an inverted gray scale. However, to compose DW images from different anatomic sections, it is important to ensure that data acquisition is performed in a way that minimizes voxel shifts between imaging stations for accurate stack alignment.

At 1.5 T, one method used to minimize stack misalignment is to omit the volume shimming at individual anatomic stations. Instead, shimming is performed at the first imaging station (e.g., head and neck area), and the same frequency offset is applied to all subsequent imaging volumes. This method minimizes voxel shifts and misalignment between imaging stations [58] without compromising image quality. However, it should be noted that this approach works well at 1.5 T but cannot be applied successfully at 3 T because the frequency-dependent voxel shift is more marked at higher field strength. At 3 T, omitting image shimming for individual stations often results in suboptimal fat suppression and

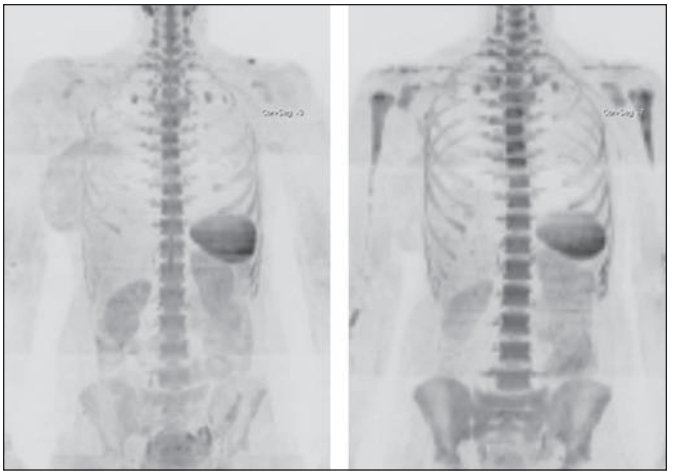

**Fig. 7**—40-year-old woman who has undergone left mastectomy and axillary nodal dissection for triple-negative breast cancer and is receiving adjuvant chemotherapy with granulocyte colony-stimulating factor (G-CSF) support. Inverted gray-scale whole-body diffusion-weighted maximum-intensity-projection images obtained before (*left*) and at 6 months after (*right*) cyclic G-CSF administration show generalized and symmetric increase in marrow signal intensity evident 6 months after treatment can mimic diffuse marrow infiltration.

substantial chemical-shift artifacts. Therefore, other solutions, including better image postprocessing, are being devised for display and analysis at 3 T.

### *Image Interpretation*

At qualitative visual appraisal of high b value images, disease is identified as areas of impeded diffusion. With inverted gray scale for image display, these areas appear as dark regions against a normal white background. Whole-body DW images should be reviewed with conventional T1-weighted or STIR or fat-suppressed T2-weighted images to ensure accurate interpretation. In oncology, DWI findings are not specific for malignancy because other cellular processes, such as inflammation, can result in similar findings. A clear clinical history should aid the weighted interpretation of abnormalities. Readers should also be aware of interpretive pitfalls, which can give rise to false-positive and false-negative results.

*False-positive findings*—The following features on whole-body DW images can be misinterpreted as disease.

Artifacts resulting from image ghosting, poor fat suppression, or susceptibility effects should not be misinterpreted as disease (Fig. 5). The clue to artifacts resulting from image ghosting and poor fat suppression is that they may appear as recapitulation of structures seen elsewhere on the image or appear at boundaries between fat and water interfaces (e.g., abdominal wall).

Normal lymph nodes return impeded diffusion to different extents during DWI. Although malignant nodes tend to have more impeded diffusion, this characteristic can be difficult to identify, particularly if the image brightness and contrast are not equalized across anatomic stations. Quantitative ADC measurements reportedly show that malignant nodes have lower ADC values than malignant lymph nodes but with substantial overlap. As such, current criteria for diagnosing nodal involvement often rely on a combination of signs, including nodal signal intensity (on its own or compared with the primary tumor), ADC value, and size criteria (short axis diameter > 1 cm).

Tiny foci (typically 1–2 mm) of impeded diffusion are sometimes detected on b value images that are difficult to correlate with structures on the corresponding T1-weighted or STIR images. Some of these foci may represent slow flow in small venules (Fig. 6). In other cases, however, the cause cannot be easily confirmed but may represent small nerves, ganglia, lymphatic vessels, blood vessels, or lymph nodes and exhibit varying degrees of impeded diffusion.

In T2 shine-through, an area of high signal intensity (or low signal intensity on the inverted gray-scale images) is visible that is not due to impeded water diffusion but is caused by the long tissue T2 relaxation time. In these cases, reviewing the corresponding ADC map would enable correct interpretation (Fig. 7). For this reason, it is recommended that

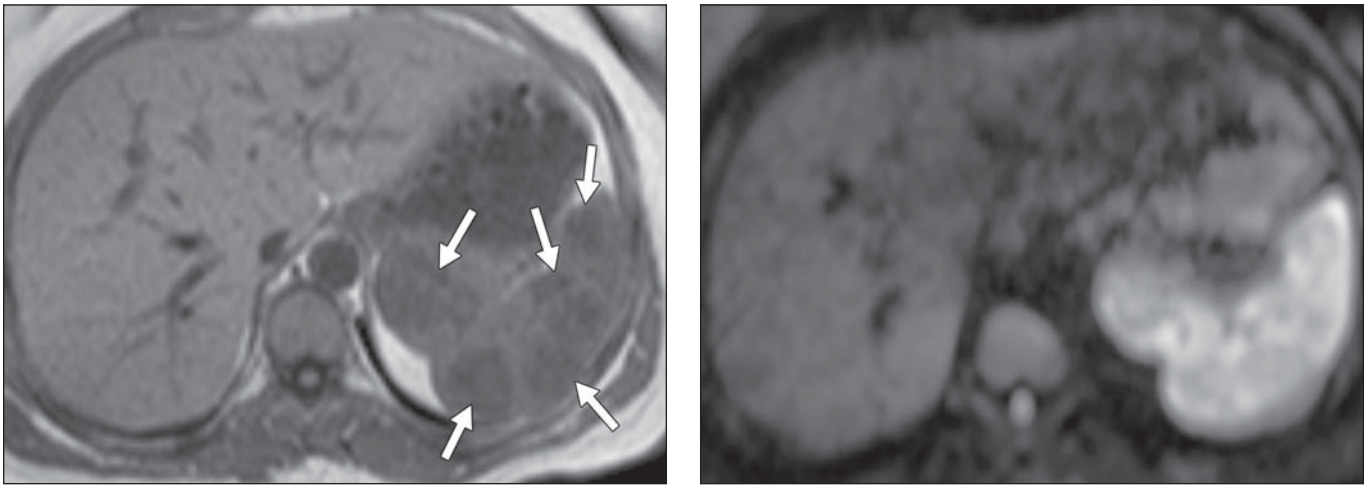

**Fig. 8**—38-year-old woman with splenic angiosarcoma. Example of possible false-negative findings.
**A,** Axial T1-weighted MR image shows several low-signal-intensity lesions (*arrows*) in spleen.
**B,** MR image (b = 750 s/mm$^2$ ) shows that lesions, because they originate in spleen, which normally exhibits impeded diffusion, appear less conspicuous.

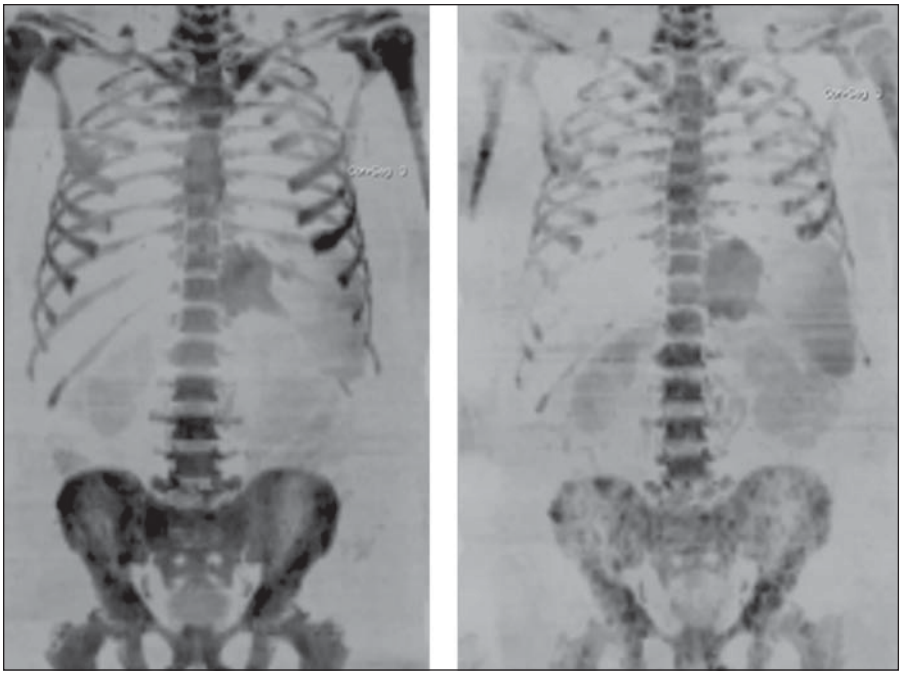

A

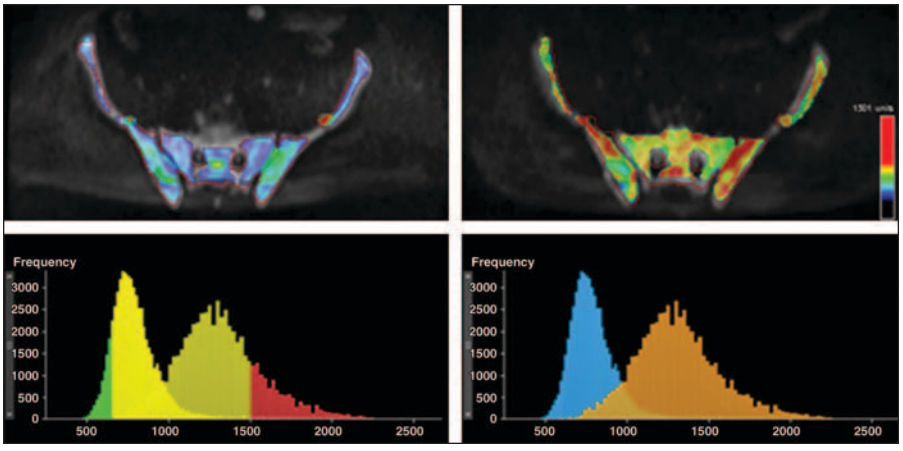


B

**Fig. 9**—54-year-old man with diffuse multiple myeloma and extraosseous myeloma in left paravertebral region. **A,** Inverted gray-scale diffusion-weighted maximum-intensity-projection images before (*left*) and 9 months after (*right*) initiation of cyclophosphamide, dexamethasone, thalidomide, and bortezomib treatment. Image 9 months after treatment shows responding disease in bony pelvis, proximal femurs, humeri, and spine. Extraosseous disease is unchanged. **B,** Apparent diffusion coefficient (ADC) histograms obtained over bony pelvis before (*left*) and after (*right*) treatment show mean ADC increase in bone disease and right shift of histogram distribution after treatment (*orange*) compared with before treatment (*blue*). Substantial proportion of voxels show increase in ADC values beyond 95th percentile of baseline histogram distribution (*red, top right*) after therapy. In lower left, yellow indicates ADC values between the 5th to 95th percentiles of the baseline distribution; green, below the 5th percentile; red, above the 95th percentile.

whole-body DWI not be performed with only a single high b value; a minimum of two b values is suggested.

A variety of nonmalignant conditions can exhibit impeded diffusion on DW images, mimicking malignant disease. Included are inflammatory conditions of the abdomen and pelvis, such as inflammatory bowel disease and abscesses. In particular, abscesses can have marked impeded water diffusion and return low ADC values [59]. However, the clinical presentation and symptoms are usually helpful in making the distinction. Diffusion marrow hyperplasia, which can occur after therapy (e.g., with granulocyte colony-stimulating factor), can cause spurious interpretation of increasing bone marrow infiltration (Fig. 8).

*False-negative findings*—Disease in normal structures can exhibit impeded water diffusion. Normal anatomic structures—such as the salivary glands, lymph nodes, spleen, spinal cord, ovaries, testes, red marrow, endometrial lining, bowel wall, peripheral nerves, and neural ganglia—have varying degrees of impeded water diffusion at DWI. As such, disease processes that originate in or involve these structures can be missed, leading to false-negative findings (Fig. 9). For this reason, whole-body DWI studies are more likely to be useful for identification of bone metastasis in older patients, in whom the paucity of normal red marrow results in better contrast between the tumor and the yellow marrow replaced by signal-suppressed fat.

Tumors that are cystic or mucinous or have an intrinsically high ADC (e.g., clear cell renal cancer) can have relative signal suppression on high b value whole-body DW images and therefore be missed. In this regard, knowledge of the clinical history is important, particularly the histologic subtype of any known malignancy at image interpretation.

Certain areas of the body are prone to imaging artifacts, which can obscure lesions. These artifacts appear in the root of the neck, the lower central mediastinum, the left lobe of the liver, and the lungs. In addition, medical implants (e.g., silicone breast implants) and orthopedic prostheses (e.g., hip and knee replacements) can result in ghosting and susceptibility artifacts. As such, lesions lying adjacent to these areas can be missed on DW images. Lesions close to metal implants may also be obscured by artifacts.

For quantitative assessment, regions of interests can be drawn on ADC maps and the tissue diffusivity recorded. Comparison of the mean or median ADC values of the same lesion before and after treatment can be used to observe tumor response as ADC changes (usually increases) after therapy. However, the measurement reproducibility of ADC values obtained with whole-body DWI technique have not been established, particularly with regard to ADC variations across anatomic imaging stations.

## Challenges

Although whole-body DWI appears highly promising, more data are needed to confirm its utility in a variety of diseases and clinical situations. There are inherent disadvantages

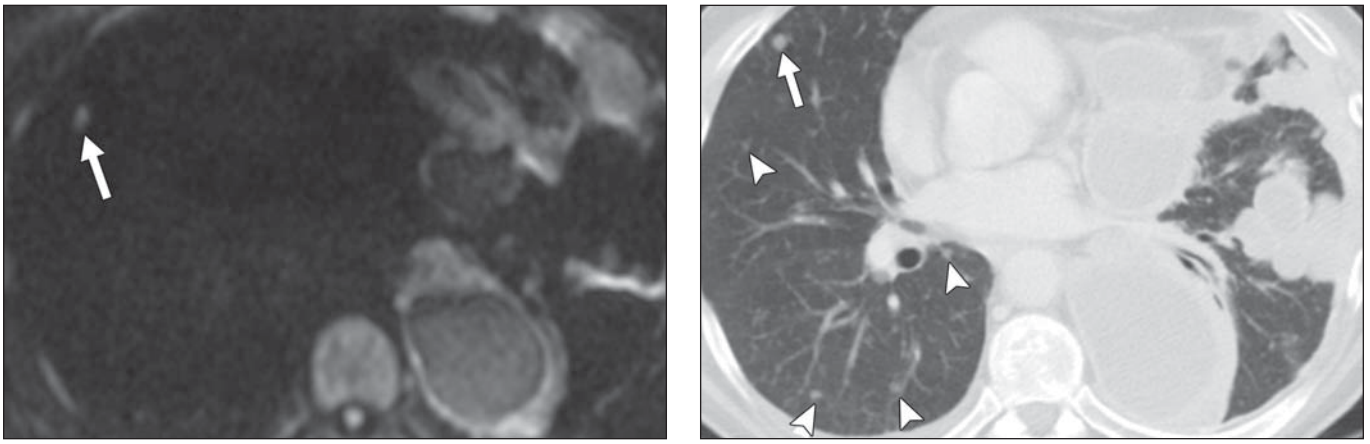

**Fig. 10**—45-year-old man with left mesothelioma.
**A,** Axial MR image (b = 750 s/mm$^2$) of thorax shows small metastatic lesion (*arrow*) in right lung.
**B,** CT image shows MRI is less sensitive than CT for detecting small metastatic lesions (*arrowheads*). Arrow indicates lesion in **A.**

of whole-body MRI, the most obvious being relative insensitivity to small lung lesions, the clinical implication of which has to be considered and debated (Fig. 10).

Accurate validation of whole-body DWI findings remains a challenge because focal features highlighted with the technique can be difficult to corroborate with findings with other imaging modalities and inaccessible for tissue sampling. When possible, a panel of reference studies, including PET, and follow-up imaging can be used for comparison. Even then, a level of uncertainty may remain regarding small lesions detected with whole-body DWI, which could require follow-up for accurate categorization.

Tools for qualitative and quantitative analysis of DW images are only beginning to emerge. Sophisticated methods are being explored to derive better descriptors of the tissue diffusion processes. The use of DWI to detect bone marrow metastasis and infiltration appears highly promising. However, more work is needed to understand how DWI signal intensity and ADC vary with age and sex in healthy persons and how these parameters change with treatment, which modulates marrow activity. There is also a need to understand the biologic variations of normal and diseased bone marrow with physiologic changes and with a range of treatments. A concerted effort in body DWI research would help to further establish the technique as an important tool in oncologic practice.

## References


1. Koh DM, Collins DJ. Diffusion-weighted MRI in the body: applications and challenges in oncology. *AJR* 2007; 188:1622–1635
2. Thoeny HC, De Keyzer F. Extracranial applications of diffusion-weighted magnetic resonance imaging. *Eur Radiol* 2007; 17:1385–1393
3. Padhani AR, Liu G, Koh DM, et al. Diffusion-weighted magnetic resonance imaging as a cancer biomarker: consensus and recommendations. *Neoplasia* 2009; 11:102–125
4. Koh DM, Takahara T, Imai Y, Collins DJ. Practical aspects of assessing tumors using clinical diffusion-weighted imaging in the body. *Magn Reson Med Sci* 2008; 6:211–224
5. Takahara T, Imai Y, Yamashita T, Yasuda S, Nasu S, Van Cauteren M. Diffusion weighted whole body imaging with background body signal suppression (DWIBS): technical improvement using free breathing, STIR and high resolution 3D display. *Radiat Med* 2004; 22:275–282
6. Steinborn MM, Heuck AF, Tiling R, Bruegel M, Gauger L, Reiser MF. Whole-body bone marrow MRI in patients with metastatic disease to the skeletal system. *J Comput Assist Tomogr* 1999; 23:123–129
7. Eustace S, Tello R, DeCarvalho V, Carey J, Melhem E, Yucel EK. Whole body turbo STIR MRI in unknown primary tumor detection. *J Magn Reson Imaging* 1998; 8:751–753
8. Lauenstein TC, Freudenberg LS, Goehde SC, et al. Whole-body MRI using a rolling table platform for the detection of bone metastases. *Eur Radiol* 2002; 12:2091–2099
9. Ghanem N, Lohrmann C, Engelhardt M, et al. Whole-body MRI in the detection of bone marrow infiltration in patients with plasma cell neoplasms in comparison to the radiological skeletal survey. *Eur Radiol* 2006; 16:1005–1014
10. Herborn CU, Unkel C, Vogt FM, Massing S, Lauenstein TC, Neumann A. Whole-body MRI for staging patients with head and neck squamous cell carcinoma. *Acta Otolaryngol* 2005; 125:1224–1229
11. Brennan DD, Gleeson T, Coate LE, Cronin C, Carney D, Eustace SJ. A comparison of whole-body MRI and CT for the staging of lymphoma. *AJR* 2005; 185:711–716
12. Engelhard K, Hollenbach HP, Wohlfart K, von Imhoff E, Fellner FA. Comparison of whole-body MRI with automatic moving table technique and bone scintigraphy for screening for bone metastases in patients with breast cancer. *Eur Radiol* 2004; 14:99–105
13. Kruger DG, Riederer SJ, Grimm RC, Rossman PJ. Continuously moving table data acquisition method for long FOV contrast-enhanced MRA and whole-body MRI. *Magn Reson Med* 2002; 47:224–231
14. Schmidt GP, Reiser MF, Baur-Melnyk A. Whole-body MRI for the staging and follow-up of patients with metastasis. *Eur J Radiol* 2009; 70:393–400
15. Börnert P, Aldefeld B. Principles of whole-body continuously-moving-table MRI. *J Magn Reson Imaging* 2008; 28:1–12
16. Han Y, Weigel M, Huff S, Ludwig U. Whole-body diffusion-weighted imaging with a continuously moving table acquisition method: preliminary results. *Magn Reson Med* 2011;
17. Bammer R. Basic principles of diffusion-weighted imaging. *Eur J Radiol* 2003; 45:169–184
18. Patterson DM, Padhani AR, Collins DJ. Technology insight: water diffusion MRI–a potential new biomarker of response to cancer therapy. *Nat Clin Pract Oncol* 2008; 5:220–233
19. Smith-Bindman R. Is computed tomography safe? *N Engl J Med* 2010; 363:1–4
20. Redberg RF. Cancer risks and radiation exposure from computed tomographic scans: how can we be sure that the benefits outweigh the risks? *Arch Intern Med* 2009; 169:2049–2050
21. Krohmer S, Sorge I, Krausse A, et al. Whole-body

MRI for primary evaluation of malignant disease in children. *Eur J Radiol* 2010; 74:256–261

22. Eisenhauer EA, Therasse P, Bogaerts J, et al. New response evaluation criteria in solid tumours: revised RECIST guideline (version 1.1). *Eur J Cancer* 2009; 45:228–247
23. Costelloe CM, Chuang HH, Madewell JE, Ueno NT. Cancer response criteria and bone metastases: RECIST 1.1, MDA and PERCIST. *J Cancer* 2010; 1:80–92
24. Krüger S, Buck AK, Mottaghy FM, et al. Detection of bone metastases in patients with lung cancer: $^{99m}$Tc-MDP planar bone scintigraphy, $^{18}$F-fluoride PET or $^{18}$F-FDG PET/CT. *Eur J Nucl Med Mol Imaging* 2009; 36:1807–1812
25. Ak I, Sivrikoz MC, Entok E, Vardareli E. Discordant findings in patients with non-small-cell lung cancer: absolutely normal bone scans versus disseminated bone metastases on positron-emission tomography/computed tomography. *Eur J Cardiothorac Surg* 2010; 37:792–796
26. Gould P. Medical isotope shortage reaches crisis level. *Nature* 2009; 460:312–313
27. Chan Y, Chan K, Lam W, Metreweli C. Comparison of whole body MRI and radioisotope bone scintigram for skeletal metastases detection. *Chin Med J (Engl)* 1997; 110:485–489
28. Imamura F, Kuriyama K, Seto T, et al. Detection of bone marrow metastases of small cell lung cancer with magnetic resonance imaging: early diagnosis before destruction of osseous structure and implications for staging. *Lung Cancer* 2000; 27:189–197
29. Mentzel HJ, Kentouche K, Sauner D, et al. Comparison of whole-body STIR-MRI and $^{99m}$Tc-methylene-diphosphonate scintigraphy in children with suspected multifocal bone lesions. *Eur Radiol* 2004; 14:2297–2302
30. Nakanishi K, Kobayashi M, Takahashi S, et al. Whole body MRI for detecting metastatic bone tumor: comparison with bone scintigrams. *Magn Reson Med Sci* 2005; 4:11–17
31. Sohaib SA, Cook G, Allen SD, Hughes M, Eisen T, Gore M. Comparison of whole-body MRI and bone scintigraphy in the detection of bone metastases in renal cancer. *Br J Radiol* 2009; 82:632–639
32. Balliu E, Boada M, Pelaez I, et al. Comparative study of whole-body MRI and bone scintigraphy for the detection of bone metastases. *Clin Radiol* 2010; 65:989–996
33. Darge K, Jaramillo D, Siegel MJ. Whole-body MRI in children: current status and future applications. *Eur J Radiol* 2008; 68:289–298
34. Ladd SC. Whole-body MRI as a screening tool? *Eur J Radiol* 2009; 70:452–462
35. Lenz C, Klarhofer M, Scheffler K, Winter L, Sommer G. Assessing extracranial tumors using diffusion-weighted whole-body MRI. *Z Med Phys* 2011; 21:79–90
36. van Ufford HM, Kwee TC, Beek FJ, et al. Newly diagnosed lymphoma: initial results with whole-body T1-weighted, STIR, and diffusion-weighted MRI compared with $^{18}$F-FDG PET/CT. *AJR* 2011; 196:662–669
37. Sommer G, Klarhofer M, Lenz C, Scheffler K, Bongartz G, Winter L. Signal characteristics of focal bone marrow lesions in patients with multiple myeloma using whole body T1w-TSE, T2w-STIR and diffusion-weighted imaging with background suppression. *Eur Radiol* 2011; 21:857–862
38. Lin C, Itti E, Luciani A, et al. Whole-body diffusion-weighted imaging with apparent diffusion coefficient mapping for treatment response assessment in patients with diffuse large B-cell lymphoma: pilot study. *Invest Radiol* 2011; 46:341–349
39. Lin C, Luciani A, Itti E, et al. Whole-body diffusion-weighted magnetic resonance imaging with apparent diffusion coefficient mapping for staging patients with diffuse large B-cell lymphoma. *Eur Radiol* 2010; 20:2027–2038
40. Laurent V, Trausch G, Bruot O, Olivier P, Felblinger J, Regent D. Comparative study of two whole-body imaging techniques in the case of melanoma metastases: advantages of multi-contrast MRI examination including a diffusion-weighted sequence in comparison with PET-CT. *Eur J Radiol* 2010; 75:376–383
41. Kwee TC, Takahara T, Vermoolen MA, Bierings MB, Mali WP, Nievelstein RA. Whole-body diffusion-weighted imaging for staging malignant lymphoma in children. *Pediatr Radiol* 2010; 40:1592–1602
42. Kwee TC, Fijnheer R, Ludwig I, et al. Whole-body magnetic resonance imaging, including diffusion-weighted imaging, for diagnosing bone marrow involvement in malignant lymphoma. *Br J Haematol* 2010; 149:628–630
43. Heusner TA, Kuemmel S, Koeninger A, et al. Diagnostic value of diffusion-weighted magnetic resonance imaging (DWI) compared to FDG PET/CT for whole-body breast cancer staging. *Eur J Nucl Med Mol Imaging* 2010; 37:1077–1086
44. Gutzeit A, Doert A, Froehlich JM, et al. Comparison of diffusion-weighted whole body MRI and skeletal scintigraphy for the detection of bone metastases in patients with prostate or breast carcinoma. *Skeletal Radiol* 2010; 39:333–343
45. Chen YB, Hu CM, Chen GL, Hu D, Liao J. Staging of uterine cervical carcinoma: whole-body diffusion-weighted magnetic resonance imaging. *Abdom Imaging* 2011; 36:619–626
46. Chen W, Jian W, Li HT, et al. Whole-body diffusion-weighted imaging vs. FDG-PET for the detection of non-small-cell lung cancer: how do they measure up? *Magn Reson Imaging* 2010; 28:613–620
47. Takenaka D, Ohno Y, Matsumoto K, et al. Detection of bone metastases in non-small cell lung cancer patients: comparison of whole-body diffusion-weighted imaging (DWI), whole-body MR imaging without and with DWI, whole-body FDG-PET/CT, and bone scintigraphy. *J Magn Reson Imaging* 2009; 30:298–308
48. Stecco A, Romano G, Negru M, et al. Whole-body diffusion-weighted magnetic resonance imaging in the staging of oncological patients: comparison with positron emission tomography computed tomography (PET-CT) in a pilot study. *Radiol Med (Torino)* 2009; 114:1–17
49. Kwee TC, van Ufford HM, Beek FJ, et al. Whole-body MRI, including diffusion-weighted imaging, for the initial staging of malignant lymphoma: comparison to computed tomography. *Invest Radiol* 2009; 44:683–690
50. Ohno Y, Koyama H, Onishi Y, et al. Non-small cell lung cancer: whole-body MR examination for M-stage assessment—utility for whole-body diffusion-weighted imaging compared with integrated FDG PET/CT. *Radiology* 2008; 248:643–654
51. Guan YJ, Ling HW, Chen KM. Preliminary application of whole body diffusion weighted imaging in screening metastasis. *Chin Med Sci J* 2008; 23:178–182
52. Nakanishi K, Kobayashi M, Nakaguchi K, et al. Whole-body MRI for detecting metastatic bone tumor: diagnostic value of diffusion-weighted images. *Magn Reson Med Sci* 2007; 6:147–155
53. Schick F. Whole-body MRI at high field: technical limits and clinical potential. *Eur Radiol* 2005; 15:946–959
54. Merkle EM, Dale BM, Paulson EK. Abdominal MR imaging at 3T. *Magn Reson Imaging Clin N Am* 2006; 14:17–26
55. Takahara T, Kwee T, Kibune S, et al. Whole-body MRI using a sliding table and repositioning surface coil approach. *Eur Radiol* 2010; 20:1366–1373
56. Ma J, Costelloe CM, Madewell JE, et al. Fast Dixon-based multisequence and multiplanar MRI for whole-body detection of cancer metastases. *J Magn Reson Imaging* 2009; 29:1154–1162
57. Nagy Z, Weiskopf N. Efficient fat suppression by slice-selection gradient reversal in twice-refocused diffusion encoding. *Magn Reson Med* 2008; 60:1256–1260
58. Li S, Sun F, Jin ZY, Xue HD, Li ML. Whole-body diffusion-weighted imaging: technical improvement and preliminary results. *J Magn Reson Imaging* 2007; 26:1139–1144
59. Dorenbeck U, Butz B, Schlaier J, Bretschneider T, Schuierer G, Feuerbach S. Diffusion-weighted echo-planar MRI of the brain with calculated ADCs: a useful tool in the differential diagnosis of tumor necrosis from abscess? *J Neuroimaging* 2003; 13:330–338
60. Fischer MA, Nanz D, Hany T, et al. Diagnostic accuracy of whole-body MRI/DWI image fusion for detection of malignant tumours: a comparison with PET/CT. *Eur Radiol* 2011; 21:246–255